TÜBİTAK

Turkish Journal of Engineering & Environmental Sciences

http://journals.tubitak.gov.tr/engineering/

Research Article

Turkish J Eng Env Sci
(2014) 38: 256 – 265

doi:10.3906/muh-1405-19

Heat transfer in oscillating hydromagnetic channel flow with arbitrary conducting walls

Khem CHAND[1,*], **Rakesh KUMAR**[2], **Sanjeev KUMAR**[1]
[1]Department of Mathematics & Statistics, H. P. University, Shimla, India
[2]Department of Mathematics, Central University, Himachal Pradesh, India

Received: 23.05.2014 • **Accepted/Published Online:** 03.04.2015 • **Printed:** 30.06.2015

Abstract: The influence of induced magnetic field and wall conductance on oscillating hydromagnetic flow of viscous incompressible electrically conducting fluid with arbitrary conducting walls in a channel has been analyzed. A uniform magnetic field H_0 is applied perpendicular to the walls. Solution of velocity field, induced magnetic, and temperature field are obtained. The numerical calculation is carried out and results are illustrated using graphs and tables.

Key words: Heat transfer, oscillating, hydromagnetic and arbitrary conductance

1. Introduction

Many transport processes exist in the geophysics, mechanical engineering, and industrial applications in which flow formation occurs in the presence of a magnetic field. The use of magnetic fluids with biological applications has become widespread and has found application in numerous biological fields like medicine, biotechnology, and diagnostics [1]. The steady laminar flow of a viscous electrically conducting fluid past a semiinfinite plate with aligned magnetic field was studied by Glauert [2] and Gribben [3] for different aspects of the flow formation. Furthermore, the unsteady boundary layer flow over a stationary semiinfinite plate in the presence of a magnetic field was studied by Ingham [4] and Takhar et al. [5] for different physical configurations. Singh and Singh [6] investigated the magnetohydrodynamic (MHD) effect on flows of viscous fluids with induced magnetic field.

The problem of the MHD flow of a viscous, incompressible, electrically conducting fluid with conducting walls has many practical applications in astrophysics, engineering, and space science. Hydromagnetic Couette flow was studied by Katagiri [7]. Chang and Yen [8] studied the effect of wall conductance. Singh and Lal [9] explored the effect of magnetic field orientation and wall conductivity on steady MHD flow. Singh and Lal [10] also studied unsteady MHD flow with arbitrary wall conductivity. Tezer-Sezgin and Dost [11] analyzed the channel flow with arbitrary wall conductivity.

The heat transfer in fluid flows has gained significance in recent times because of its applications in recent advancements of space technology. For example the aerodynamic heat transfer around high-speed vehicles has importance in the present era with the advent of rocketry and supersonic flights. The velocity distribution in the flow field and the study of the thermal boundary layer along with the influence of different forces (or kinematical factors) on this boundary layer is a major aspect of heat transfer problems. The heat transfer in MHD channel flow was discussed by Yen [12], Soundalgekar [13], and Jagdeesan [14].

*Correspondence: khemthakur99@gmail.com

The induced magnetic field has many important applications in the experimental and theoretical studies of MHD flow due to its use in many scientific and technological phenomena. In this paper, we have analyzed the effect of an induced magnetic field and wall conductance on the oscillating hydromagnetic flow of viscous, incompressible, and electrically conducting fluid with arbitrary conducting walls.

2. Mathematical formulation

Consider the oscillatory MHD flow of viscous, incompressible, and electrically conducting fluid confined between two infinite conducting walls separated by distance 2L as in Figure 1. The origin is assumed to be at the middle of the channel, the x-axis is taken in the direction of the flow, and the y-axis is perpendicular to it. A uniform magnetic field H_0 is applied perpendicular to the walls. Since the walls are infinite along the x-axis, all the physical quantities depend only on y and t. The fluid through the conducting walls is governed by following equations

$$\frac{\partial u^*}{\partial t^*} = -\frac{1}{\rho}\frac{\partial p^*}{\partial x^*} + \nu\frac{\partial^2 u^*}{\partial y^{*2}} + \frac{\mu_e H_0}{4\pi\rho}\frac{\partial H_x^*}{\partial y^*}, \tag{1}$$

$$\frac{\partial H^*}{\partial t^*} = H_0\frac{\partial u^*}{\partial y^*} + \eta\frac{\partial^2 H_x^*}{\partial y^{*2}}, \tag{2}$$

$$\rho C_p\frac{\partial T^*}{\partial t^*} = \kappa\frac{\partial^2 T^*}{\partial y^{*2}} + \mu\left(\frac{\partial u^*}{\partial y^*}\right)^2 + \frac{1}{\sigma}\left(\frac{\partial H_x^*}{\partial y^*}\right)^2, \tag{3}$$

where ρ is the density of the fluid, ν is the kinematic viscosity, μ_e is the magnetic permeability, η is the resistivity, C_p is the specific heat at constant pressure, κ is the thermal conductivity, μ is the coefficient of viscosity, and σ is the electrical conductivity of the fluid.

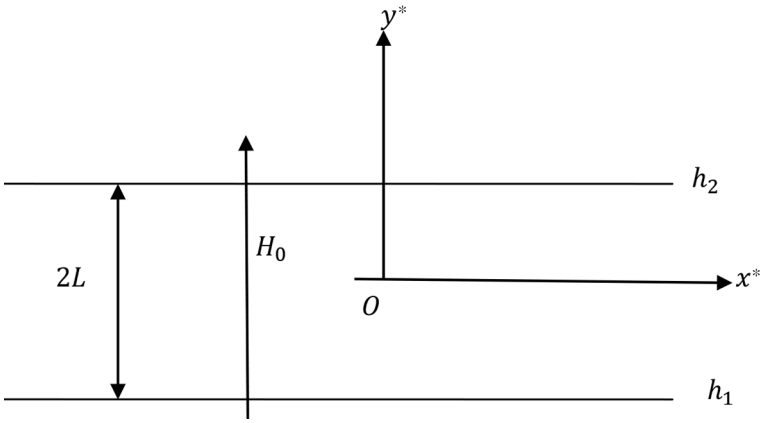

Figure 1. Geometrical configuration of the problem.

The boundary conditions are:

$$\left.\begin{array}{l} u^* = \frac{\partial H_x^*}{\partial y^*} - \frac{\sigma H_x^*}{\sigma_1 h_1} = 0,\ T^* = T_1^* \text{ at } y^* = -L \\ and \\ u^* = \frac{\partial H_x^*}{\partial y^*} + \frac{\sigma H_x^*}{\sigma_2 h_2} = 0,\ T^* = T_2^* \text{ at } y^* = L \end{array}\right\}. \tag{4}$$

We assume the flow under the influence of the pressure gradient in the X^*-axis of the following form:

$$-\frac{1}{\rho}\frac{\partial P^*}{\partial x^*} = A(1+\in e^{i\omega^* t^*}), \tag{5}$$

where A is the amplitude of the pressure gradient and $\in$ is the small perturbation parameter.

To solve Eqs. (1), (2), and (3), we assume that:

$$u^* = u_0^* + \in u_1^* e^{i\omega^* t^*},\ H_x^* = H_{x_0}^* + \in H_{x_1}^* e^{i\omega^* t^*},\ T^* = T_0^* + \in T_1^* e^{i\omega^* t^*} \in < 1. \tag{6}$$

Substituting Eqs. (5) and (6) into Eqs. (1), (2), and (3), and equating the harmonic and nonharmonic parts and neglecting the coefficient of $\in^2$, we get the following equations:

$$0 = A + \nu \frac{d^2 u_0^*}{dy^{*2}} + \frac{\mu_e H_0}{4\pi\rho} \frac{dH_{x_0}^*}{dy^*} \tag{7}$$

$$0 = H_0 \left(\frac{du_0^*}{dy^*} \right) + \eta \frac{d^2 H_{x_0}^*}{dy^{*2}} \tag{8}$$

$$0 = \kappa \frac{d^2 T_0^*}{dy^{*2}} + \mu \left(\frac{du_0^*}{dy^*} \right)^2 + \frac{1}{\sigma} \left(\frac{dH_{x_0}^*}{dy^*} \right)^2 \tag{9}$$

$$i\omega^* u_1^* = A + \nu \frac{d^2 u_1^*}{dy^{*2}} + \frac{\mu_e H_0}{4\pi\rho} \frac{dH_{x_1}^*}{dy^*} \tag{10}$$

$$i\omega^* H_{x_1}^* = H_0 \frac{du_1^*}{dy^*} + \eta \frac{d^2 H_{x_1}^*}{dy^{*2}} \tag{11}$$

$$\rho C_p i\omega^* t^* T_1^* = \kappa \frac{d^2 T_1^*}{dy^{*2}} + 2\mu \left(\frac{du_0^*}{dy^*} \right) \left(\frac{du_1^*}{dy^*} \right) + \frac{2}{\sigma} \left(\frac{dH_{x_0}^*}{dy^*} \right) \left(\frac{dH_{x_1}^*}{dy^*} \right) \tag{12}$$

The boundary conditions are transformed to:

$$\left.\begin{array}{l} u_0^* = u_1^* = \frac{dH_{x_0}^*}{\partial y^*} - \frac{\sigma H_{x_0}^*}{\sigma_1 h_1} = \frac{dH_{x_1}^*}{\partial y^*} - \frac{\sigma H_{x_1}^*}{\sigma_1 h_1} = 0, T_0^* = T_1, T_1^* = 0 \text{ at } y^* = -L \\ \text{and} \\ u_0^* = u_1^* = \frac{dH_{x_0}^*}{dy^*} + \frac{\sigma H_{x_0}^*}{\sigma_2 h_2} = \frac{dH_{x_1}^*}{dy^*} + \frac{\sigma H_{x_1}^*}{\sigma_2 h_2} = 0, T_0^* = T_2, T_1^* = 0 \text{ at } y^* = L \end{array}\right\}, \tag{13}$$

where σ_1, σ_2, h_1, and h_2 are the electrical conductivity and thickness of the upper and lower plates, respectively.

We introduce the following nondimensional quantities:

$$y = \frac{y^*}{L},\quad u_0 = \frac{u_0^*}{A^*},\quad u_1 = \frac{u_1^*}{A^*},\quad H_{x_0} = \frac{H_{x_0}^*}{H_0 R_m},\quad H_{x_1} = \frac{H_{x_1}^*}{H_0 R_m}, \theta_0 = \frac{T_0^* - T_1}{T_2 - T_1}, \theta_1 = \frac{T_1^* - T_1}{T_2 - T_1},\quad A^* = \frac{AL^2}{\nu},$$

$\omega = \frac{\omega^* L^2}{\nu}$, $R_m = 4\pi\mu_e \sigma L A^*$ is the magnetic Reynolds number, $R_e = \frac{LA^*}{\nu}$ is the Reynolds number, $M^2 = \frac{\mu_e^2 H_0^2 L^2 \sigma}{\mu}$ is the Hartmann number, $P_r = \frac{C_p \mu}{\kappa}$ is the Prandtl number, $P_m = \sigma\mu_e\nu$ is the magnetic Prandtl number, and $E_c = \frac{A^2 L^2}{\nu^2 C_{P(T_2 - T_1)}}$ is the Eckert number.

Using the above non dimensional parameters in Eqs. (7)–(12), we get the following nondimensional equations.

$$\frac{d^2 u_0}{dy^2} + M^2 \frac{dH_{x_0}}{dy} = -1 \tag{14}$$

$$\frac{d\partial^2 H_{x_0}}{dy^2} + \frac{du_0}{dy} = 0 \tag{15}$$

$$\frac{d^2 u_1}{dy^2} + M^2 \frac{dH_{x_1}}{dy} + 1 = i\omega u_1 \tag{16}$$

$$\frac{d^2 H_{x_1}}{dy^2} + \frac{du_1}{dy} = i\omega \frac{R_m}{R_e} H_{x_1} \tag{17}$$

$$\frac{d^2\theta_0}{dy^2} = -P_r E_c \left(\left(\frac{du_0}{dy} \right)^2 + \left(\frac{MR_m}{P_m R_e} \right)^2 \left(\frac{dH_{x_0}}{dy} \right)^2 \right) \tag{18}$$

$$\frac{d^2\theta_1}{dy^2} - i\omega P_r \theta_1 = -2P_r E_c \left(\left(\frac{du_0}{dy} \right) \left(\frac{du_1}{dy} \right) + \left(\frac{MR_m}{P_m R_e} \right)^2 \left(\frac{dH_{x_0}}{dy} \right) \left(\frac{dH_{x_1}}{dy} \right) \right) \tag{19}$$

The boundary conditions in nondimensional form become:

$$\left.\begin{array}{l} u_0 = u_1 = \frac{dH_{x_0}}{dy} - \frac{1}{\phi_1} H_{x_0} = 0, \frac{dH_{x_1}}{dy} - \frac{1}{\phi_1} H_{x_1} = \theta_0 = \theta_1 = 0 \text{ at } y = -1 \\ and \\ u_0 = u_1 = \frac{dH_{x_0}}{dy} + \frac{1}{\phi_2} H_{x_0} = 0, \frac{dH_{x_1}}{dy} + \frac{1}{\phi_2} H_{x_1} = 0, \theta_0 = 1, \theta_1 = 0 \,\text{at}\, y = 1 \end{array}\right\}, \tag{20}$$

where $\phi_1 = \frac{\sigma_1 h_1}{\sigma L}$ and $\phi_2 = \frac{\sigma_2 h_2}{\sigma L}$ are the dimensionless wall conductance ratios.

The solutions of Eqs. (14)–(19) under the boundary conditions of Eq. (20) are as follows.

$$u_0 = \frac{(2\phi + \phi_4\phi_5)\,(coshM - coshMy)}{M\,(2M\phi coshM + \phi_4\phi_5 sinhM)} \tag{21}$$

$$H_{x_0} = \frac{(2\phi + \phi_4\phi_5)}{M^2\,(2M\phi coshM + \phi_4\phi_5 sinhM)} \left(sinhMy + \frac{\phi_3}{\phi} sinhM \right) - \frac{1}{M^2} \left(\frac{\phi_3}{\phi} - y \right) \tag{22}$$

$$\begin{aligned} \theta_0 \;=\; & \frac{E_c P_r A_1^2}{4} \left[\frac{1}{2M^2} \left\{ 1 + \left(\frac{R_m}{R_e P_m} \right)^2 \right\} (cosh2M - cosh2My) + \frac{1}{2M^3} \left(\frac{R_m}{R_e P_m} \right)^2 (coshM - coshMy) \right. \\ & \left. + \left(\frac{R_m}{R_e P_m} \right)^2 \left\{ \left(1 + \frac{2}{M^2} \right) - 1 \right\} (1 - y^2) \right] \end{aligned} \tag{23}$$

$$u_1 = c_1\beta e^{b_1 y} - c_2\beta e^{-b_1 y} + c_3\gamma e^{b_2 y} - c_4\gamma e^{-b_2 y} + A \tag{24}$$

$$H_{x1} = c_1 e^{b_1 y} + c_2 e^{-b_1 y} + c_3 e^{b_2 y} + c_4 e^{-b_2 y} \tag{25}$$

$$\begin{aligned} \theta_1 \;=\; & c_5 coshry + c_6 sinhry + 2E_c P_r A_1 \left[A_2 \left(c_1 e^{(M+b_1)y} - c_2 e^{-(M+b_1)y} \right) \right. \\ & + A_3 \left(c_2 e^{(M-b_1)y} - c_1 e^{-(M-b_1)y} \right) + A_4 \left(c_3 e^{(M+b_2)y} - c_4 e^{-(M+b_2)y} \right) \\ & \left. + A_5 \left(c_4 e^{(M-b_2)y} - c_3 e^{-(M-b_2)y} \right) - A_6 \left(c_1 e^{b_1 y} - c_2 e^{-b_1 y} \right) - A_7 \left(c_3 e^{b_2 y} - c_4 e^{-b_2 y} \right) \right] \end{aligned} \tag{26}$$

3. Results and discussion

To study the effect of Reynolds number, magnetic Reynolds number, Hartmann number, wall conductance, Prandtl number, magnetic Prandtl number, Eckert number, and frequency of oscillations on MHD flow, numerical calculation has been carried out and the results are exhibited graphically in Figures 2–13.

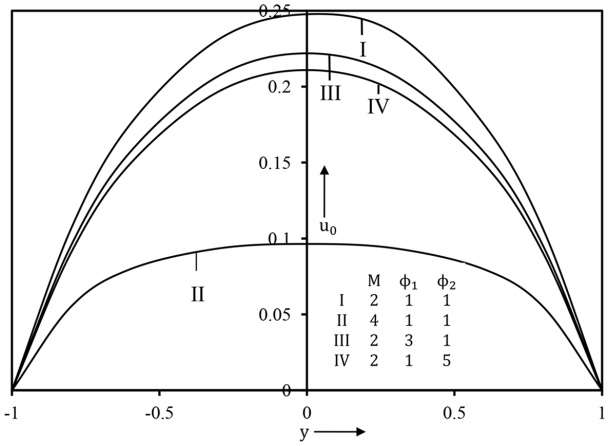

Figure 2. Steady velocity profile $\mathbf{u_0}$.

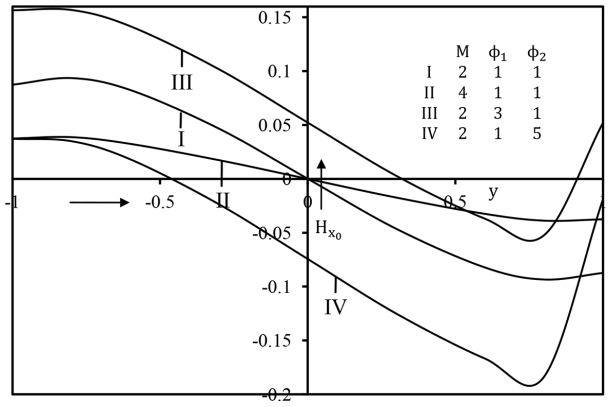

Figure 3. Steady induced magnetic field $\mathbf{H_{x_0}}$.

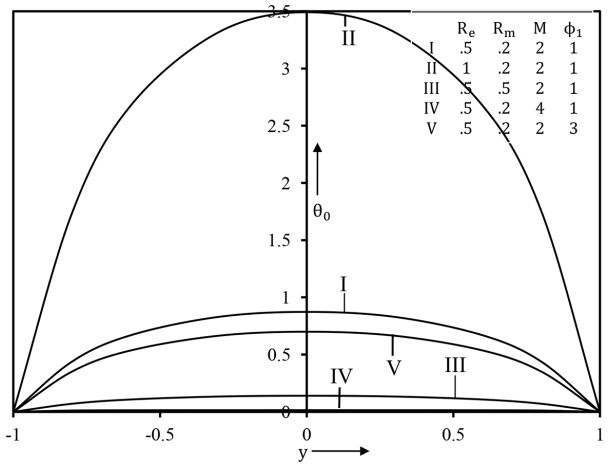

Figure 4. Steady temperature Profile θ_0 for $\phi_2 = 1$, $\mathbf{P_r = 0.7, P_m = 0.1}$, and $\mathbf{E_c = 2}$.

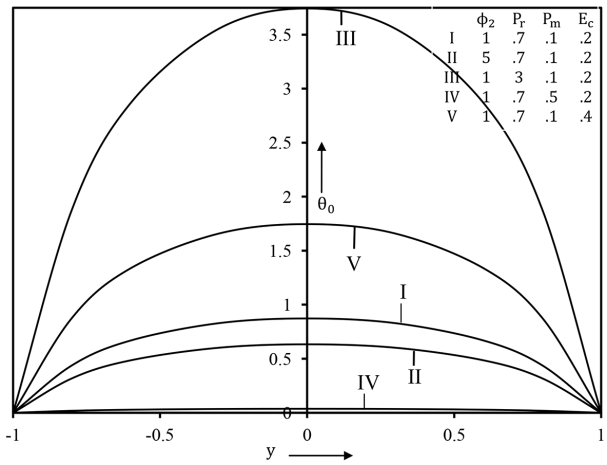

Figure 5. Steady temperature Profile θ_0 for $\mathbf{R_e = 0.5}$, $\mathbf{R_m = 0.5, M = 2}$, and $\phi_1 = 1$.

The steady part of the velocity is presented in Figure 2; velocity is maximum along the middle of the channel and decreases with the increase of Hartmann number and wall conductance of the lower and upper walls of the channel.

The steady part of the induced magnetic field is presented in Figure 3, where it is clear that the magnitude of induced magnetic field increases as we move towards the lower wall and decreases with the increase of Hartmann number in the lower half while it increases in the upper half of the channel. The magnitude of induced magnetic field increases with the increase of lower wall conductance and deceases with the increase of upper wall conductance.

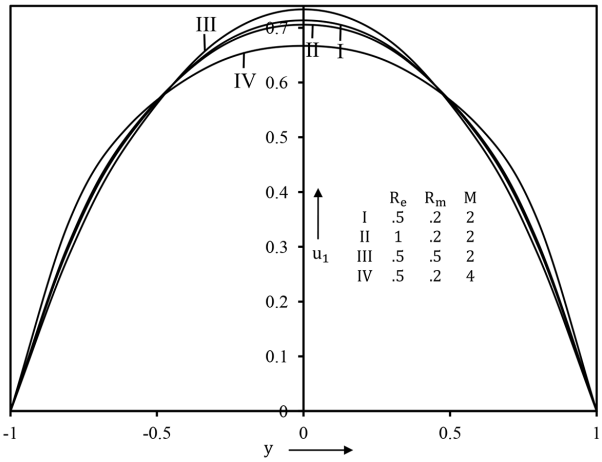

Figure 6. Unsteady velocity profile u_1 for $\phi_1 = 1$, $\phi_2 = 1$, and $\omega = 5$.

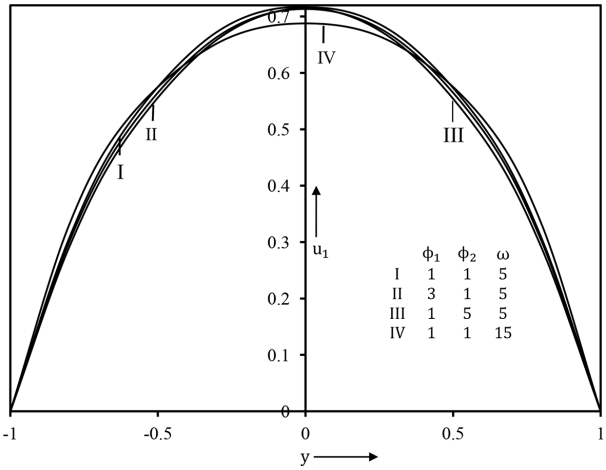

Figure 7. Unsteady velocity profile u_1 for $R_e = 0.5$, $R_m = 0.5$, and $M = 2$.

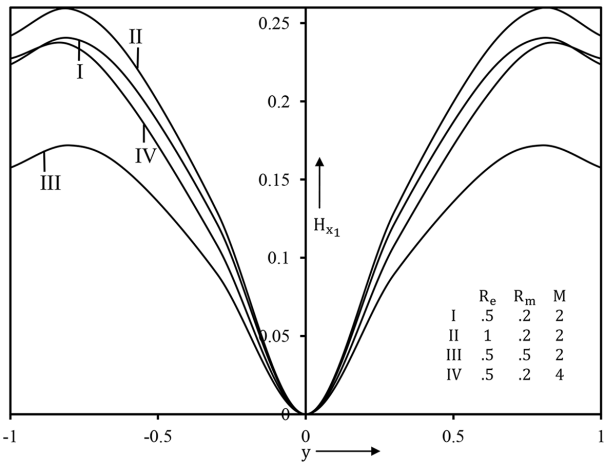

Figure 8. Unsteady induced magnetic field profile H_{x1} for $\phi_1 = 1$, $\phi_2 = 1$, and $\omega = 5$.

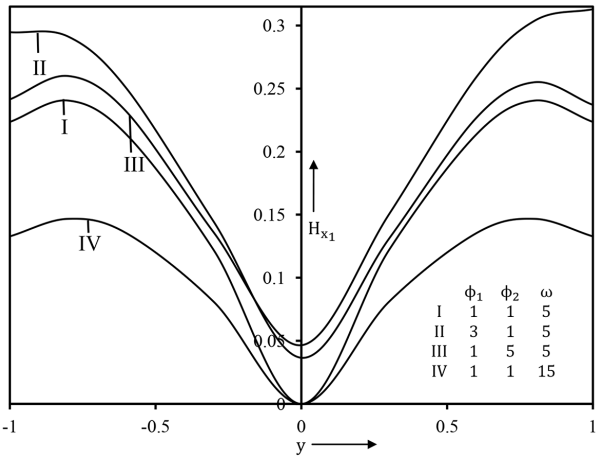

Figure 9. Unsteady induced magnetic field profile H_{x1} for $R_e = 0.5$, $R_m = 0.5$, and $M = 2$.

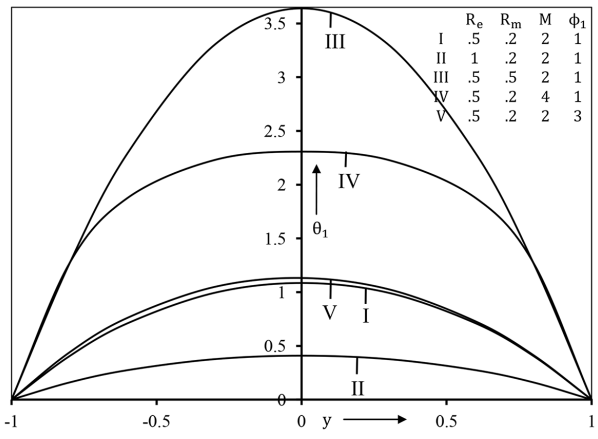

Figure 10. Unsteady temperature profile θ_1 for $\phi_2 = 1$, $\mathbf{P_r = 0.7, P_m = 0.1, E_c = 0.2}$, and $\omega = 5$.

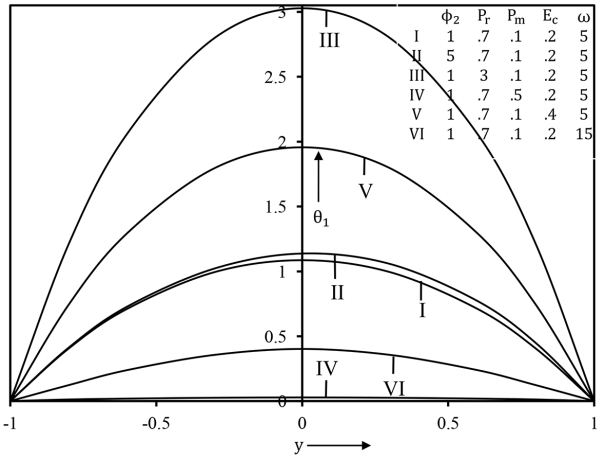

Figure 11. Unsteady temperature profile θ_1 for $\mathbf{R_e = 0.5}$, $\mathbf{R_m = 0.5, M = 2}$, and $\phi_1 = 1$.

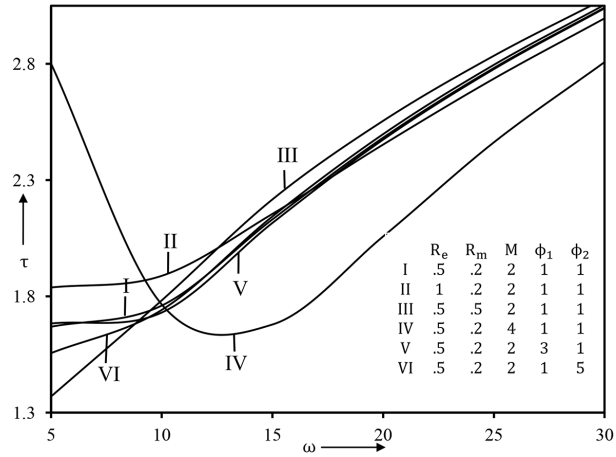

Figure 12. Unsteady shear stress at the upper wall ($y = 1$) of the channel.

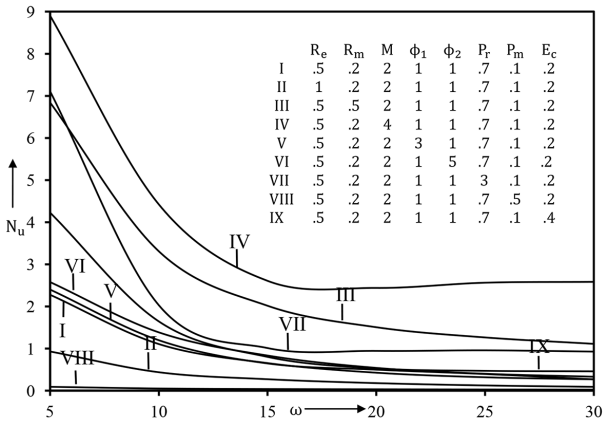

Figure 13. Unsteady rate of heat transfer.

The steady part of the temperature profile is presented in Figures 4 and 5, where with the increase in Reynolds number, Prandtl number, and Eckert number the temperature of the fluid increases, while all other parameters decrease the temperature of the fluid.

Steady shear stress at the lower wall ($y = -1$) and upper wall ($y = 1$) of the channel is given by:

$$\left(\frac{du_0}{dy}\right)_{y=\mp 1} = \frac{\pm\left(2\phi + \phi_4\phi_5\right) sinhM}{\left(2M\phi coshM + \phi_4\phi_5 sinhM\right)}. \tag{27}$$

The numerical values of steady shear stress at the lower wall ($y = -1$) and upper wall ($y = 1$) are presented in Table 1. Shear stresses decrease with increase of the Hartmann number and wall conductance at the lower wall and increase at the upper wall of the channel.

Table 1. Steady shear stress at lower and upper wall of the channel.

M	ϕ_1	ϕ_2	$y = -1$	$y = 1$
2	1	1	0.65048	-0.65048
4	1	1	0.39979	-0.39979
2	3	1	0.52861	-0.52861
2	1	5	0.55372	-0.55372

Steady rate of heat transfer at the lower wall ($y = -1$) and upper wall ($y = 1$) of the channel is given by the following.

$$\begin{aligned}\left(\frac{d\theta_0}{dy}\right)_{y=\mp 1} = & -\frac{E_c P_r A_1^2}{4}\left[\frac{1}{2M^2}\left\{1+\left(\frac{R_m}{R_e P_m}\right)^2\right\}(2M cosh 2M)\right. \\ & \left. +\frac{1}{2M^2}\left(\frac{R_m}{R_e P_m}\right)^2 (coshM) \mp 2\left(\frac{R_m}{R_e P_m}\right)^2\left\{\left(1+\frac{2}{M^2}\right)-1\right\}\right]\end{aligned} \tag{28}$$

The numerical values of the steady rate of heat transfer at the lower wall ($y = -1$) and upper wall ($y = 1$) are presented in Table 2, depicting that the steady rate of heat transfer decreases with increase of the Reynolds

number, Prandtl number, and Eckert number and increases with all other parameters at both the lower and upper wall of the channel.

Table 2. Steady rate of heat transfer at lower wall ($y = 1$) and upper wall ($y = 1$) of the channel.

R_e	R_m	M	ϕ_1	ϕ_2	P_r	P_m	E_c	$y = -1$	$y = 1$
0.5	0.2	2	1	1	0.7	0.1	0.2	–1.9613	–3.0157
1	0.2	2	1	1	0.7	0.1	0.2	–7.8322	–12.053
0.5	0.5	2	1	1	0.7	0.1	0.2	–0.3175	–0.4853
0.5	0.2	4	1	1	0.7	0.1	0.2	–0.1091	–0.1104
0.5	0.2	2	3	1	0.7	0.1	0.2	–1.5734	–2.4192
0.5	0.2	2	1	5	0.7	0.1	0.2	–1.4212	–1.5734
0.5	0.2	2	1	1	3	0.1	0.2	–8.4058	–12.924
0.5	0.2	2	1	1	0.7	0.5	0.2	–0.0827	–0.1238
0.5	0.2	2	1	1	0.7	0.1	0.4	–3.923	–6.0314

The unsteady velocity profile is shown graphically in Figures 6 and 7. Clearly, the unsteady velocity is maximum along the middle of the channel. It increases with increase of Reynolds number, Hartmann number, and frequency of oscillations near the lower and upper wall and decreases in the middle of the channel, with an opposite effect for the magnetic Reynolds number. It is also observed that unsteady velocity profile decreases near the lower wall while it increases near the upper wall with the increase of lower wall conductance, whereas upper wall conductance has the reverse effect.

The unsteady part of the induced magnetic field is shown graphically in Figures 8 and 9. Its magnitude is minimum at the middle of the channel and it increases with Reynolds number and lower and upper wall conductance while it decreases with increase of the magnetic Reynolds number, Hartmann number, and frequency of oscillations

The variation in unsteady temperature profile is presented graphically in Figures 10 and 11. It is evident that unsteady temperature profile increases with Reynolds number, magnetic Prandtl number, and frequency of oscillations, while it increases with the increase of all other parameters.

Unsteady shear Stress at the upper wall $(y = 1)$ of the channel is given by:

$$\left(\frac{du_1}{dy}\right)_{y=1} = c_1 b_1 \beta e^{b_1} + \beta b_1 e^{-b_1} + c_3 \gamma b_2 e^{b_2} + c_4 \gamma b_2 e^{-b_2}.$$

The unsteady shear stress at the upper wall of the channel is presented graphically in Figure 12. The unsteady shear stress increases with frequency of oscillations, Reynolds number, magnetic Reynolds number, and upper wall conductance while it decreases with Hartmann number and lower wall conductance of the channel.

Unsteady rate of heat transfer at the upper wall $(y = 1)$ of the channel is given by the following.

$$\begin{aligned}\left(\frac{d\theta_1}{dy}\right)_{y=1} &= c_5 r cosh r + c_6 r sinh r + 2E_c P_r A_1 \Big[A_2 (M+b_1)\left(c_1 e^{(M+b_1)} + c_2 e^{-(M+b_1)}\right) \\ &+ A_3 (M-b_1)\left(c_2 e^{(M-b_1)} + c_1 e^{-(M-b_1)}\right) + A_4 (M+b_2)\left(c_3 e^{(M+b_2)} + c_4 e^{-(M+b_2)}\right) \\ &+ A_5 (M-b_2)\left(c_4 e^{(M-b_2)} + c_3 e^{-(M-b_2)}\right) - A_6 b_1 \left(c_1 e^{b_1} + c_2 e^{-b_1}\right) - A_7 b_2 \left(c_3 e^{b_2} + c_4 e^{-b_2}\right)\Big] \quad (29)\end{aligned}$$

The unsteady rate of heat transfer is presented graphically in Figure 13. It is evident that unsteady rate of heat transfer decreases with the frequency of oscillations, Reynolds number, lower wall conductance, and magnetic Prandtl number, while it increases with the increase of all other parameters.

Additional information is available in the Appendix (on the journal's website).

4. Conclusions

The main conclusions of this study are as follows:

1. The steady part of the induced magnetic field increases as we move towards the lower wall and decreases with the increase of Hartmann number in the lower half while it increases in the upper half of the channel. It also increases with the increase of lower wall conductance and deceases with the increase of upper wall conductance. While the unsteady part of the induced magnetic field is minimum along the middle of the channel, it increases with lower and upper wall conductance and decreases with Hartmann number.

2. The maximum velocity is along the middle of the channel, and the steady part of the velocity profile decreases with the increase of Hartmann number while the unsteady part of velocity shows a reverse effect. The steady part of the velocity profile decreases with the conductance of the lower and upper walls of the channel. It is also observed that unsteady velocity profile decreases near the lower wall while increasing near the upper wall with the increase of lower wall conductance, whereas upper wall conductance has the opposite effect.

Acknowledgment

The authors are thankful to the learned referees for their valuable suggestions and technical comments.

Appendix

$$\phi=\frac{1}{\phi_1}+\frac{1}{\phi_2},\quad \phi_3=\frac{1}{\phi_1}-\frac{1}{\phi_2},\quad \phi_4=\phi+\phi_3,\quad \phi_5=\phi-\phi_3,\quad \alpha=M^2+i\omega\left(N+1\right),\quad r=\sqrt{i\omega P_r}.$$

$$b_1=\frac{1}{\sqrt{2}}\left[\alpha+\left(\alpha^2+4\omega^2\frac{R_e}{R_m}\right)^{\frac{1}{2}}\right]^{\frac{1}{2}},\quad b_2=\frac{1}{\sqrt{2}}\left[\alpha-\left(\alpha^2+4\omega^2\frac{R_e}{R_m}\right)^{\frac{1}{2}}\right]^{\frac{1}{2}},\quad \beta=\frac{i\omega N-b_1^2}{b_1},\quad \gamma=\frac{i\omega N-b_2^2}{b_2},$$

$$A_1=\frac{2\phi+\phi_4\phi_5}{2M\phi coshM+\phi_4\phi_5 SinhM},\quad A_2=\frac{\left(i\omega N-b_1^2\right)-\frac{R_e^2}{R_m^2P_m^2}b_1M}{\left(M+b_1\right)^2-r^2},\quad A_3=\frac{\left(i\omega N-b_1^2\right)+\frac{R_e^2}{R_m^2P_m^2}b_1M}{\left(M-b_1\right)^2-r^2},$$

$$A_4=\frac{\left(i\omega N-b_2^2\right)-\frac{R_e^2}{R_m^2P_m^2}b_2M}{\left(M+b_2\right)^2-r^2},\quad A_5=\frac{\left(i\omega N-b_2^2\right)+\frac{R_e^2}{R_m^2P_m^2}b_2M}{\left(M-b_2\right)^2-r^2},\quad A_6=\frac{R_e^2}{R_m^2P_m^2}\frac{b_1}{\left(b_1^2-r^2\right)},\quad A_7=\frac{R_e^2}{R_m^2P_m^2}\frac{b_2}{\left(b_2^2-r^2\right)}.$$

References

[1] Ramchand CN, Pande P, Kapcansky P, Mehta R V. Application of magnetic fluids in medicine and biotechnology. Indian J Pure Ap Phy 2001; 39: 683–686.

[2] Glauert MB. A study of the MHD boundary layer on a flat plate. J Fluid Mech 1961; 10: 276–288.

[3] Gribben RJ. The MHD boundary layer in the presence of a pressure gradient. P R Soc London 1965; 287: 123–141.

[4] Ingham DB. Flow past an impulsively started semi-infinite flat plate in the presence of a magnetic field. IMA J Appl Math 1977; 20: 459–469.

[5] Takhar HS, Chamkha AJ, Nath G. Unsteady flow and heat transfer on a semi-infinite flat plate with an aligned magnetic field. Int J Eng Sci 1999; 37: 1723–1736.

[6] Singh NP, Singh AK. MHD effects on flow of viscous fluid with induced magnetic field. Indian J Pure Ap Phy 2001; 39: 240–245.

[7] Katagiri M. Flow formation in Couette motion in magnetohydrodynamics. J Phys Soc Jpn 1962; 17: 393–396.

[8] Chang CC, Yen JT. Magnetodynamics channel flow as influenced by wall conductance. ZAMP 1962; 13: 266–272.

[9] Singh B, Lal J. Effect of magnetic field orientation and wall conductivity on MHD channel flow using finite element method. Comput Method Appl M 1983; 40: 159–169.

[10] Singh B, Lal J. Finite element method for unsteady MHD flow through pipes with arbitrary wall conductivity. Int J Numer Meth Fl 1984; 4: 291–302.

[11] Tezer-Sezgin M, Dost S. Boundary element method for MHD channel flow with arbitrary wall conductivity. Appl Math Model 1994; 18: 429–436.

[12] Yen JT. Effect of electrical conductance on MHD heat transfer in a channel. J Heat Transf-T ASME 1963; 85: 371–377.

[13] Soundalgekar VM. On heat transfer in crossed fluid MHD channel flow between conducting walls. P Natl Inst Sci India 1959; 35: 329.

[14] Jagdeesan K. Heat Transfer due to hydromagnetic channel flow with conducting walls. AIAA J 1964; 2: 756-762.